


ORIGINAL ARTICLE

Photonic devices fabricated from (111)-oriented single crystal diamond

Blake Regan¹ | Sejeong Kim¹ | Anh T. H. Ly¹ | Aleksandra Trycz¹ |
Kerem Bray¹ | Kumaravelu Ganesan² | Milos Toth¹ | Igor Aharonovich¹ 

¹School of Mathematical and Physical Sciences, University of Technology Sydney, Ultimo, New South Wales, Australia

²School of Physics, University of Melbourne, Melbourne, Victoria, Australia

Correspondence

Igor Aharonovich, School of Mathematical and Physical Sciences, University of Technology Sydney, Ultimo 2007, New South Wales, Australia.
Email: igor.aharonovich@uts.edu.au

Funding information

Office of Naval Research Global; Research and Development; Australian Research Council, Grant/Award Numbers: DP180100077, DP190101058

Abstract

Diamond is a material of choice in the pursuit of integrated quantum photonic technologies. So far, the majority of photonic devices fabricated from diamond are made from (100)-oriented crystals. In this work, we demonstrate a methodology for the fabrication of optically active membranes from (111)-oriented diamond. We use a liftoff technique to generate membranes, followed by chemical vapor deposition of diamond in the presence of silicon to generate homogenous silicon vacancy color centers with emission properties that are superior to those in (100)-oriented diamond. We further use the diamond membranes to fabricate microring resonators with quality factors exceeding ~3000. Supported by finite-difference time-domain calculations, we discuss the advantages of (111)-oriented structures as building blocks for quantum nanophotonic devices.

KEYWORDS

cavity, color centers, diamond

Diamond is an attractive platform for studies of light-matter interaction at the nanoscale.¹⁻⁷ In the past decade, defects in diamond, also known as color centers, have emerged as attractive candidates for scalable solid-state quantum photonic architectures.^{1,6} While earlier works were focused predominantly on nitrogen vacancy (NV) centers,^{8,9} recent effort is devoted to group IV defects,¹⁰⁻¹⁵ (eg, the silicon vacancy [SiV]) due to their narrowband emission and a better resilience to electromagnetic fluctuations.

Integration of these color centers with photonic resonators is an important challenge for several reasons. First, it enables enhancement of the photon emission flux from the single color centers (for instance by using diamond pillars¹⁶). Second, it provides the means to

interconnect potential quantum nodes in a large network, where the emitters are coupled to individual cavities and interconnected with a waveguide.^{17,18} Finally, if the photonic resonator is carefully designed with coupled directional emission, one can achieve high cavity cooperativity and realize advanced quantum phenomena such as single photon switch with a solid-state system.¹⁹ However, despite the remarkable progress in nanofabrication of diamond cavities,^{8,20} all photonic resonators to date were fabricated from (100)-oriented diamond, primarily because this is the most common orientation provided by commercial suppliers and the difficulty in engineering and polishing (111)-oriented crystals.²¹ This, however, limits the potential coupling strength of many color centers to cavities, since most centers studied to date have

This is an open access article under the terms of the Creative Commons Attribution License, which permits use, distribution and reproduction in any medium, provided the original work is properly cited.

© 2020 The Authors. *InfoMat* published by John Wiley & Sons Australia, Ltd on behalf of UESTC.

dipoles oriented along the $\langle 111 \rangle$ direction, and the dipole overlap with the cavity field is therefore not optimal in cavities fabricated from (100)-oriented diamond. Conversely, in (111)-oriented diamond, the overlap is optimal, and superior Purcell enhancement is expected.

In the current work, we fabricated large area (111) diamond membranes that exhibit bright SiV luminescence. Consequently, these membranes were utilized to engineer diamond microring resonators with quality factors of ~ 3000 . Our work launches a new approach for the fabrication of diamond devices with different crystallographic orientations.

The fabrication process begins with (111)-oriented single crystal diamond (obtained from New Diamond Technology). Single-crystal membranes were fabricated by helium ion implantation (1 MeV He⁺ ions, dose of 5×10^{16} ions/cm²) followed by an electrochemical liftoff

process.^{22,23} Figure 1A shows an optical image of a diamond membrane after liftoff. In many cases, the shape of the membrane is defined by the (111) orientation in the face centered cubic structure, characterized by a cleavage angle of $\sim 60^\circ$. Figure 1B shows a scanning electron microscope (SEM) image of a different diamond membrane.

The membranes are then transferred onto a silicon substrate and overgrown using a microwave plasma chemical vapor deposition (MPCVD) system to introduce SiV centers.²⁴ The MPCVD growth conditions are as follows: a hydrogen/methane ratio of 100:1 at 60 Torr, a microwave power of 900 W, and a growth time of 10 minutes. Figure 1C shows an overgrown diamond membrane, with a smooth, single crystal surface.

To confirm the (111) membrane orientation, X-ray diffraction (XRD) and electron backscattered diffraction

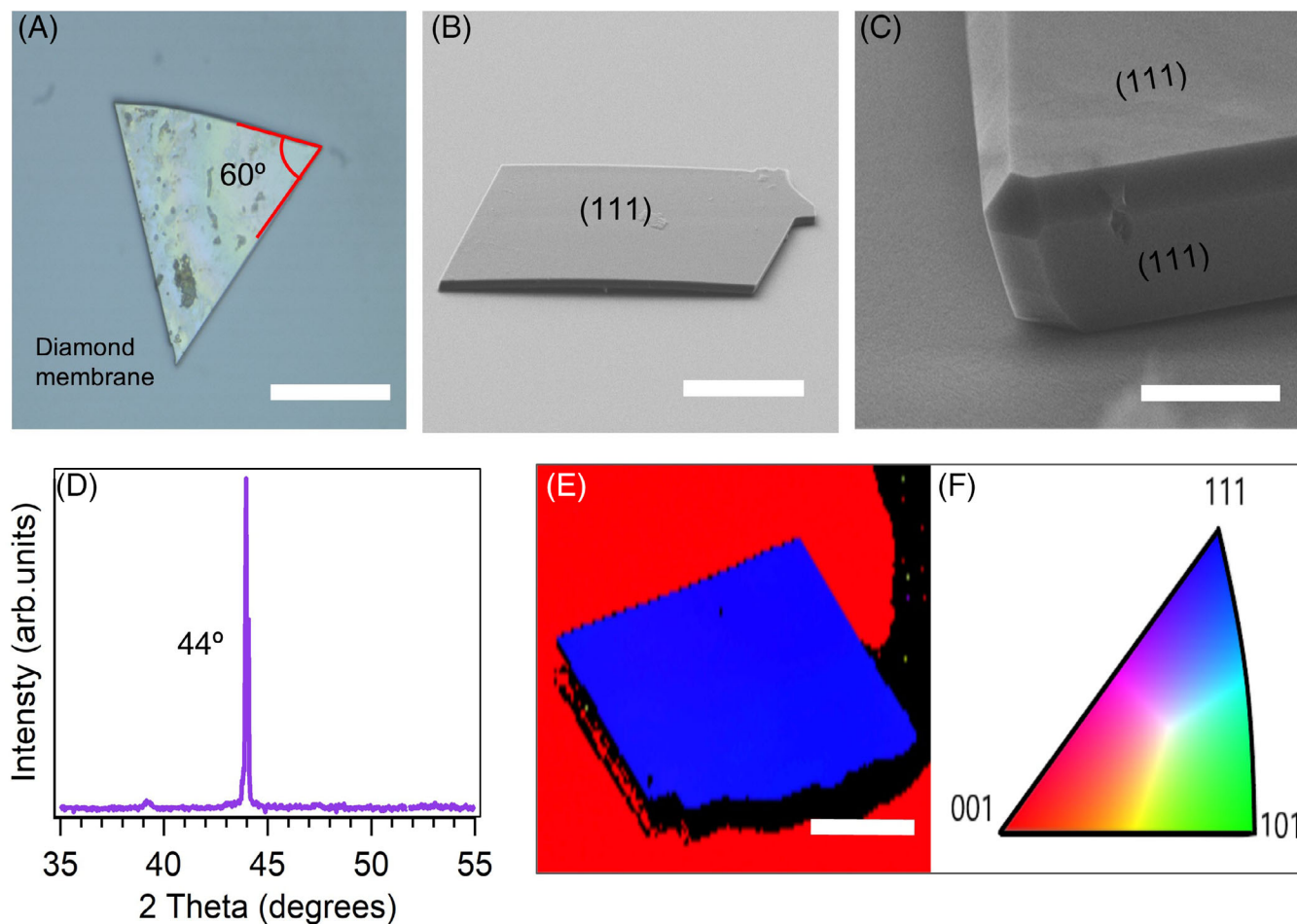


FIGURE 1 Single crystal (111) diamond membranes. A, Optical image of a (111) membrane showing triangular cleaving angle, marked at $\sim 60^\circ$. B, SEM image in tilted view showing a (111) membrane. C, Magnified view of a membrane edge after CVD overgrowth. The scale bar corresponds to 1 μm . D, X-ray diffraction (XRD) spectrum showing a peak at 44° , characteristic of a (111)-orientated crystal. E, EBSD map of a (111)-oriented, overgrown diamond membrane (blue). The red background is (001)-oriented silicon, and the dark regions are amorphous PMMA. The image was taken at an electron beam incidence angle of 70° . The scale bars in A, B, and E correspond to 100 μm . CVD, chemical vapor deposition; PMMA, poly-methyl methacrylate; SEM, scanning electron microscope

(EBSD) analyses were performed. Figure 1D shows an XRD spectrum of the original bulk single crystal diamond with a pronounced peak at $2\theta = 44^\circ$, confirming the (111) orientation of the crystal.²¹ Figure 1E shows an EBSD map recorded from the overgrown membrane, confirming further that it is single crystal (111)-oriented diamond through analysis of kikuchi pattern information derived from back scattering of electrons in SEM.

A comparison of (111)- and (100)-oriented membranes was performed to demonstrate the advantages of the former. A (111)-oriented diamond membrane and a similarly sized (100)-membrane were situated on a silicon substrate $\sim 100\ \mu\text{m}$ apart. Both membranes were cleaned in piranha solution prior to fabrication. The membranes were overgrown simultaneously using the MPCVD conditions detailed earlier in order to incorporate SiV color centers (see Figure 2A,B). Each membrane was subsequently flipped and thinned down to 300 nm using inductively coupled plasma-reactive ion etching (ICP-RIE), and their thickness was confirmed with high angle SEM analysis. Note that the original diamond that was subject to He ion implantation is fully removed, and the final devices are made only from the pristine, overgrown diamond. The primary cause for interference pattern in Figure 2B is the thin-film effect of the $\sim 300\ \text{nm}$ diamond membranes on the substrate. The fringes are caused by residual liquid trapped between the membrane and the substrate and the different adhesions in the different spots. This is confirmed by moving the membrane and observing a change in fringes.

The thinned membranes were subsequently examined by photoluminescence (PL) spectroscopy. While the intensity at the edge of each membrane was comparable, line scans (Figure 2C) across the membranes show a clear difference in PL homogeneity. The average PL intensity from the (111)-oriented membrane (Figure 2A) is more intense, and the line profile is more uniform. The (100) membrane, on the other hand, (Figure 2B) showed a significantly higher intensity reduction moving inward from the edges of the membrane. PL spectra from both membranes are shown in Figure 2D,E, showing a prominent SiV emission with a zero phonon line at 738 nm. Given the similar thicknesses of the membranes after the thinning step, the difference in PL intensity is attributed to a better incorporation of the SiV into the growing (111)-oriented diamond membrane. Similar results were obtained previously for the NV centers in diamond that showed to preferentially incorporate into (111) grown diamonds.²⁵⁻²⁸ The edges of both membranes have similar PL intensities since a (100)-oriented membrane has a (111) facet at the edge due to the three dimensional single crystal diamond growth. Both membranes do experience a drop-off in intensity toward the center of the membrane, this can be attributed to scattering enhancement at the edges and losses into bulk material.

To provide more insight into the coupling efficiency between the emitters in diamond membrane and the cavity modes, we perform a finite-difference time-domain simulation. We focus here on the group IV defects, and

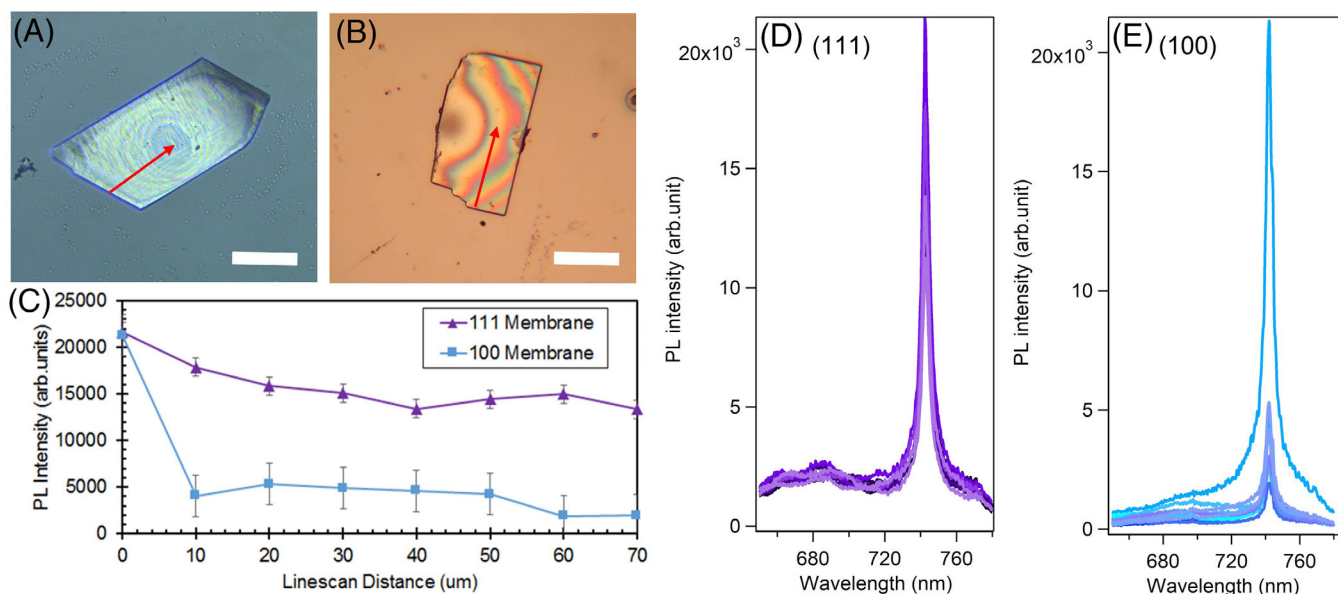


FIGURE 2 Homogeneous distribution of SiV centers in a 111-oriented diamond membrane. Optical images showing (A) a (111) diamond membrane and (B) (100) diamond membrane. Scale bars correspond to $50\ \mu\text{m}$. Red arrows indicate line scan direction and length used for (D) and (E). C, PL intensity vs distance for (111)- and (100)-oriented membranes. Photoluminescence spectra collected along the line scans from the (111)-oriented membrane (D) and (100)-oriented membrane (E). PL, photoluminescence

predominantly the SiV defect. Its structure is a split vacancy with a silicon in an interstitial location along the $\langle 111 \rangle$ symmetry axis, resulting in a D_{3d} point group symmetry. Figure 3A shows the schematic drawing of the four (i, ii, iii, and iv) potential orientations of SiV defect in a (111)-oriented diamond.^{29,30} These orientations are further simplified with red arrows indicating dipole orientations and α indicating angles between the dipole and the $\langle 111 \rangle$ vector. One SiV dipole orientation is perpendicular to the surface, while the rest of the dipoles make equal angle of 70.5° with the top diamond surface. The same SiV dipole in (100) membrane would form an angle of 54.7° . In our study, dipole orientations for the three out of the four (111) directions within the diamond membrane are almost parallel to the membrane. Therefore, our approach is advantageous for TE-like cavity modes, but will play little advantage for the TM mode. Indeed, most of the photonic cavities are designed for transverse electric (TE)-like modes, meaning dipoles with larger angle α would have a better electric field overlap. Consequently, Purcell factor with respect to the dipole angle α is calculated as shown in Figure 3B for a diamond microring. The simulation result shows that more in-plane components dipole has the higher Purcell factor is expected. Note that we conducted simulation for SiV center in this case, but this would be true also for other group IV defects in diamond.

Given the advantages of the (111) membranes, ring resonators have been engineered from this material. Electron beam lithography was employed to pattern a hydrogen silsesquioxane (HSQ) layer spuncoat onto the diamond membrane, forming an SiO_2 hard mask array of microring resonators with ring radius of $5 \mu\text{m}$ and

waveguide width of 400 nm . The pattern is transferred into the diamond membrane through a second ICP-RIE step with Oxygen at 10 mTorr . Finally, the mask is removed with another RIE step of SF_6 at 40 mTorr to directly etch the SiO_2 mask and undercut into the SiO_2 substrate. Figure 4A shows the SEM of the patterned microrings, while Figure 4B shows a high-resolution image of an individual microring. The top roughness is relatively negligible and the postprocessing roughness matches the roughness of the original membrane ($<5 \text{ nm RMS}$). The roughness caused by the mask removal is predominantly on the side walls of the resonators. This roughness is caused by the walls of the mask material etching at a higher rate than the bulk of the mask. From our SEM images, the roughness is estimated at $\sim 20 \text{ nm}$.

The diamond cavities were then probed using a green laser in a standard confocal microscope. Figure 4C shows the whispering gallery modes from the resonator (manifested by the periodic peaks in the spectrum). With the designated microring size, the free spectral range should be $\sim 14 \text{ nm}$. The spectrum of the ring resonators is augmented by the modes of the optical cavity surrounding the SiV peak at $\sim 738 \text{ nm}$. Figure 4C further shows that an emission enhancement forms the fabricated microring cavities as compared with the membrane. An enhancement of ~ 25 times is observed after measuring a number of devices.

A high-resolution spectrum centered at the SiV region is shown in Figure 4D. Quality factors as high as ~ 3000 were observed from these devices (measured as $\lambda/\Delta\lambda$). The losses occur due to an increased roughness from the imperfect HSQ mask removal and from the leakage to the underlying SiO_2 substrate. The enhancement of

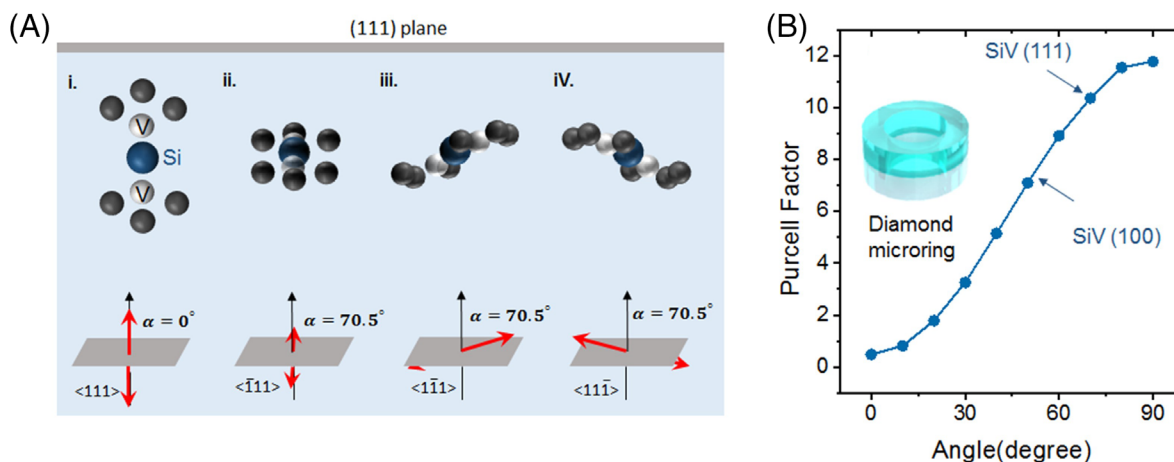


FIGURE 3 Dipole orientation in (111)-oriented diamond and Purcell factors. A, Simplified schematics of the four possible orientations of SiV centers in (111)-oriented diamond and the corresponding dipole orientations (red arrows). The angle α between the $\langle 111 \rangle$ direction and the dipole is shown in each case. B, Calculated Purcell factor as a function of a dipole angle with respect to the top surface of the ring. SiV, silicon vacancy

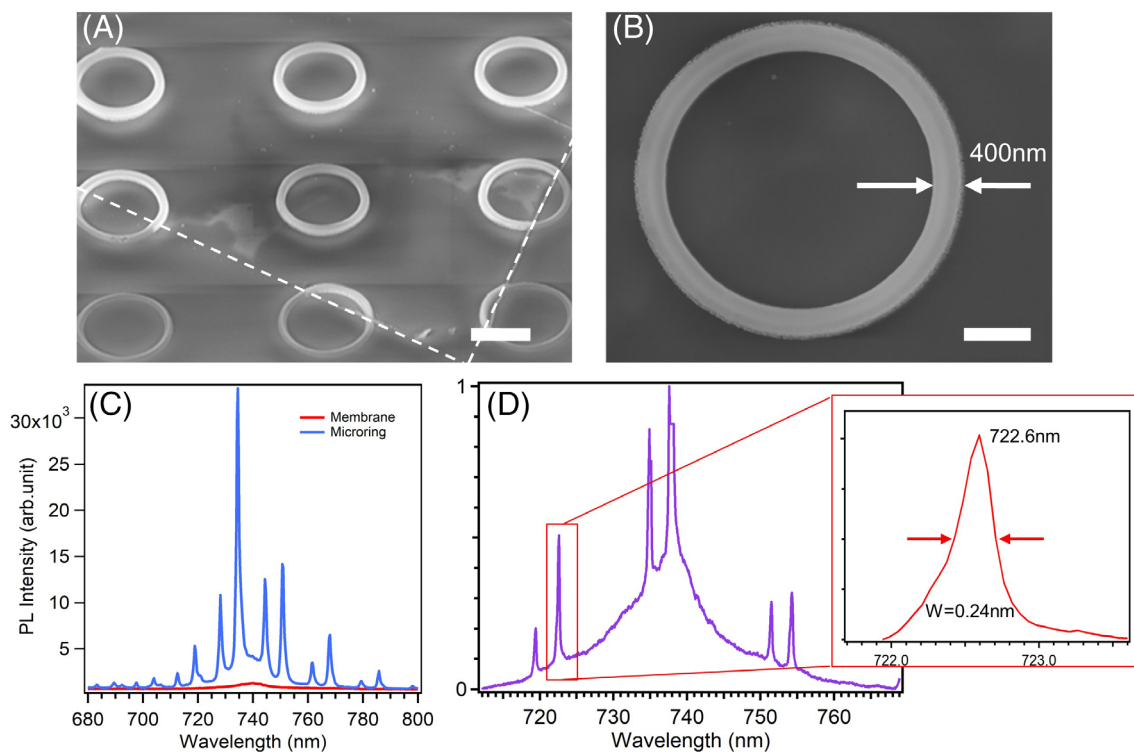


FIGURE 4 Diamond ring resonators fabricated from (111) diamond membrane containing SiV color centers. A, A wide area at 45° inclination depicting the array of microrings. The dotted line is the membrane boundary; scale bar corresponds to 3 μm . B, A top view of an individual microring; scale bar correlates to 1 μm . C, PL spectrum recorded from the diamond microring cavity under 532 nm excitation at room temperature. WGMs are clearly visible. The zero phonon line of the SiV center is observed at 738 nm. Comparison of recorded emission from SiV color center recorded from the membrane and from a microring cavity, showing an enhancement of ~ 25 times. D, Fine grating spectral analysis of whispering gallery resonators, individual marked mode with FWHM of ~ 0.24 nm, Q factor ~ 3000 . FWHM, full width at half maximum; SiV, silicon vacancy; WGM, whispering gallery mode

brightness from the optically active diamond resonators is desirable for the application of color centers to integrated nanophotonic devices.

In conclusion, we have described a robust method to engineer high-quality single crystal diamond membranes from (111)-oriented diamond. The improved brightness in (111)-oriented membranes is favorable for sensing applications—particularly for NV-based magnetometry, and for photonic devices with group IV color centers. Furthermore, we have demonstrated the use of this platform for the fabrication of ring resonators with quality factors up to ~ 3000 , supported by a theoretical model that confirms a higher Purcell enhancement for the (111)-oriented devices. Similar techniques can be explored to achieve doping of (111) diamond membranes with other group IV emitters,¹⁵ or other emerging color centers in diamond. Furthermore, our work may also pave way to free-standing mechanical cantilevers from (111) diamond membranes for new generation of diamond micro- and nano-electromechanical systems.³¹ Our results will accelerate the integration of diamond with scalable photonic devices to achieve on-chip quantum nanophotonic circuitry.

ACKNOWLEDGMENTS

We thank Dr Carlo Bradac for useful discussions and Dr Mark Lockrey for assistance with the EBSD data. Financial support from the Australian Research Council (via DP180100077 and DP190101058), the Asian Office of Aerospace Research and Development (grant FA2386-17-1-4064), and the Office of Naval Research Global (grant N62909-18-1-2025).

CONFLICT OF INTEREST

The authors declare no conflict of interest.

ORCID

Igor Aharonovich  <https://orcid.org/0000-0003-4304-3935>

REFERENCES

- Atatüre M, Englund D, Vamivakas N, Lee S-Y, Wrachtrup J. Material platforms for spin-based photonic quantum technologies. *Nature Rev Materials*. 2018;3:38-51.
- Schröder T, Mouradian SL, Zheng J, et al. Quantum nanophotonics in diamond [Invited]. *J Opt Soc Am B*. 2016;33:B65-B83.

3. Aharonovich I, Greentree AD, Praver S. Diamond photonics. *Nat Photonics*. 2011;5:397-405.
4. Lenzini F, Gruhler N, Walter N, Pernice WHP. Diamond as a platform for integrated quantum photonics. *Adv Quantum Technol*. 2018;1:1800061.
5. Eaton SM, Hadden JP, Bharadwaj V, et al. Quantum micro-nano devices fabricated in diamond by femtosecond laser and ion irradiation. *Adv Quantum Technol*. 2019;2:1970033.
6. Awschalom DD, Hanson R, Wrachtrup J, Zhou BB. Quantum technologies with optically interfaced solid-state spins. *Nat Photonics*. 2018;12:516-527.
7. Radulaski M, Zhang JL, Tzeng Y-K, et al. Nanodiamond integration with photonic devices. *Laser Photonics Rev*. 2019;13:1800316.
8. Hausmann BJM, Shields BJ, Quan Q, et al. Coupling of NV centers to photonic crystal nanobeams in diamond. *Nano Lett*. 2013;13:5791-5796.
9. Bernien H, Hensen B, Pfaff W, et al. Heralded entanglement between solid-state qubits separated by three metres. *Nature*. 2013;497:86-90.
10. Evans RE, Bhaskar MK, Sukachev DD, et al. Photon-mediated interactions between quantum emitters in a diamond nanocavity. *Science*. 2018;362:662-665.
11. Schröder T, Trusheim ME, Walsh M, et al. Scalable focused ion beam creation of nearly lifetime-limited single quantum emitters in diamond nanostructures. *Nat Commun*. 2017;8:15376.
12. Becker JN, Pingault B, Groß D, et al. All-optical control of the silicon-vacancy spin in diamond at millikelvin temperatures. *Phys Rev Lett*. 2018;120:053603.
13. Sun S, Zhang JL, Fischer KA, et al. Cavity-enhanced Raman emission from a single color center in a solid. *Phys Rev Lett*. 2018;121:083601.
14. Zhou Y, Rasmita A, Li K, Xiong Q, Aharonovich I, Gao W-B. Coherent control of a strongly driven silicon vacancy optical transition in diamond. *Nat Commun*. 2017;8:14451.
15. Bradac C, Gao WB, Forneris J, Trusheim ME, Aharonovich I. Quantum nanophotonics with group IV defects in diamond. *Nat Commun*. 2019;10:5625.
16. Neu E, Appel P, Ganzhorn M, et al. Photonic nanostructures on (111)-oriented diamond. *Appl Phys Lett*. 2014;104:153108.
17. Wehner S, Elkouss D, Hanson R. Quantum internet: a vision for the road ahead. *Science*. 2018;362:303.
18. Wang J, Paesani S, Ding Y, et al. Multidimensional quantum entanglement with large-scale integrated optics. *Science*. 2018;360:285-291.
19. Sun S, Kim H, Luo Z, Solomon GS, Waks E. A single-photon switch and transistor enabled by a solid-state quantum memory. *Science*. 2018;361:57-60.
20. Khanaliloo B, Mitchell M, Hryciw AC, Barclay PE. High-Q/V monolithic diamond microdisks fabricated with quasi-isotropic etching. *Nano Lett*. 2015;15:5131-5136.
21. Parks SM, Grote RR, Hopper DA, Bassett LC. Fabrication of (111)-faced single-crystal diamond plates by laser nucleated cleaving. *Diam Relat Mater*. 2018;84:20-25.
22. Magyar A.; Lee J. C.; Limarga A. M.; Aharonovich I.; Rol F.; Clarke D. R.; Huang M. B.; Hu E. L., Fabrication of thin, luminescent, single-crystal diamond membranes *Appl Phys Lett* 2011;99:081913-3.
23. Bray K, Regan B, Trycz A, et al. Single crystal diamond membranes and photonic resonators containing germanium vacancy color centers. *ACS Photonics*. 2018;5:4817-4822.
24. Lee JC, Aharonovich I, Magyar AP, Rol F, Hu EL. Coupling of silicon-vacancy centers to a single crystal diamond cavity. *Opt Express*. 2012;20:8891-8897.
25. Tallaire A, Collins AT, Charles D, et al. Characterisation of high-quality thick single-crystal diamond grown by CVD with a low nitrogen addition. *Diam Relat Mater*. 2006;15:1700-1707.
26. Fukui T, Doi Y, Miyazaki T, et al. Perfect selective alignment of nitrogen-vacancy centers in diamond. *Appl Phys Express*. 2014;7:055201.
27. Michl J, Teraji T, Zaiser S, et al. Perfect alignment and preferential orientation of nitrogen-vacancy centers during chemical vapor deposition diamond growth on (111) surfaces. *Appl Phys Lett*. 2014;104:102407.
28. Osterkamp C, Mangold M, Lang J, et al. Engineering preferentially-aligned nitrogen-vacancy Centre ensembles in CVD grown diamond. *Sci Rep*. 2019;9:5786.
29. Rogers L. J.; Jahnke K. D.; Doherty M. W.; Dietrich A.; McGuinness L. P.; Müller C.; Teraji T.; Sumiya H.; Isoya J.; Manson N. B.; Jelezko F., Electronic structure of the negatively charged silicon-vacancy center in diamond. *Phys Rev B* 2014;89:235101.
30. Lesik M, Plays T, Tallaire A, et al. Preferential orientation of NV defects in CVD diamond films grown on (113)-oriented substrates. *Diam Relat Mater*. 2015;56:47-53.
31. Wu H, Sang L, Li Y, et al. Reducing intrinsic energy dissipation in diamond-on-diamond mechanical resonators toward one million quality factor. *Phys Rev Mater*. 2018;2:090601.

How to cite this article: Regan B, Kim S, Ly ATH, et al. Photonic devices fabricated from (111)-oriented single crystal diamond. *InfoMat*. 2020;2:1241-1246. <https://doi.org/10.1002/inf2.12090>